# Assessment of the Flexural Behavior of Reinforced Concrete Beams Strengthened with Concrete Jackets

M. Monir A. Alhadid[1], Maged A. Youssef, P.Eng.[2]

[1] PhD Candidate, E-mail: majjanal@uwo.ca, [2] Professor, E-mail: youssef@uwo.ca

Department of Civil and Environmental Engineering, Western University, London, ON, Canada N6A5B9

**Abstract:**

Analysis of continuous jacketed Reinforced Concrete (RC) beams requires accounting for the nonlinear behavior of the interface and the materials as well as redistribution of moments. This kind of analysis is complex and require an advanced level of knowledge and experience to perform. Engineers need simplified yet robust tools to practically predict the actual behavior of jacketed RC beams. In the current practice, slip is neglected in the analysis and monolithic behavior is assumed for the jacketed section, which result in higher estimates of stiffness and/or capacity. This paper provides a simplified method to analyze continuous jacketed RC beams taking into account the interfacial slip distribution and the actual nonlinear behavior of both concrete and steel. An iterative calculation algorithm is developed to determine the moment-curvature curves of a jacketed beam at different sections. The developed method allows the evaluation of interfacial slip and shear stress distributions in ductile reinforced concrete beams. The developed method is utilized to conduct an extensive parametric study, which resulted into modification factors that can be used to calculate the capacity and deformations of a strengthened beam considering the interfacial slip.

**Keywords:** Reinforced Concrete; Continuous; Jacketing; Slip; Interface; Monolithic Factors; Inelasticity; Flexure.

## 1. Introduction

The need to strengthen Reinforced Concrete (RC) structures emerges from various reasons, such as new safety requirements, a change of structure occupancy, an incorrect design calculations and/or degradation of materials with time. Jacketing is one of the widely spread procedures to strengthen and repair RC beams. It comprises the addition of concrete layers that are usually reinforced with longitudinal steel bars, stirrups, welded wire mesh or various kinds of fibrous materials.

In the current practice, monolithic action is assumed between the original beam and the attached jacket. This implies that the internal stresses developed in both substrates due to the applied loads are distributed among them assuming infinite interfacial slip stiffness. This assumption may result in higher estimates of stiffness and/or capacity depending on the geometrical properties and interfacial surface treatment. The actual behavior of typical jacketed beams is partially composite and depends on the frictional resistance between the surfaces and the presence of steel anchors connecting the two substrates [1]. This implies that the analysis of jacketed beams requires a knowledge of the nonlinear behavior of the interface as well as the nonlinear properties of both concrete and the embedded steel bars at each loading step along the beam.

Literature is ample with experimental programs and numerical investigations that have been performed to address the influence of jacketing schemes, geometrical characteristics, mechanical properties and interfacial treatment on the flexural behavior of determinate jacketed RC structural members. For instance, Altun [2] and Bousias *et al.* [3] examined the effect of RC jacketing on the mechanical performance of statically-determinate RC beams considering the load-displacement behavior, ultimate load, ductility and toughness. Other researchers [1, 4] investigated the

1 significance of surface preparation of concrete members before applying the new concrete jacket.
2 The use of fiber reinforced cementitious composites as an alternative to adding steel reinforcement
3 within the jacket has been addressed by other studies [5 – 10]. In addition, the impact of using
4 shear studs to further attach the existing beam with the additional concrete layers has been
5 investigated by Shehata *et al.* [11]. Furthermore, the influence of varying the method of applying
6 the jacket on site, such as shotcrete or cast-in-place concrete, have been considered by many
7 researchers [12, 13, 14].

8 Experimental and numerical studies related to strengthening indeterminate RC beams using
9 concrete jackets is scarce in literature. At the time of writing, the only available relevant
10 experimental work was performed by Cheong and MacAlevey [15]. The rather extensive use of
11 indeterminate RC beams in building structures and bridges requires further research regarding the
12 influence of partial composite action their flexural performance.

13 This paper is a continuation of an ongoing research [16], which aims at proposing a simplified
14 method to capture the influence of interfacial slip on the moment-curvature ($M$-$\varphi$) and load-
15 deflection ($P$-$\Delta$) relationships of jacketed continuous RC beams. This is achieved by performing
16 nonlinear analysis in view of the material properties and interfacial behavior. A calculation
17 algorithm is proposed to determine the slip distribution along the beam length and to obtain the
18 corresponding $M$-$\varphi$ diagram at both the sagging and hogging moment regions. This analysis
19 procedure is sensitive to the bending moment distribution along the beam; therefore, the concept
20 of moment redistribution in indeterminate beams is illustrated and considered in the analysis. The
21 validated model is used to perform a parametric study aiming at examining the flexural behavior
22 of the strengthened beams. Finally, a regression analysis is performed to propose slip modification
23 factors that can be used to obtain the actual $M$-$\varphi$ diagram of continuous RC beams considering

interfacial slip. The scope of the proposed work is limited to ductile RC beams by considering sufficient reinforcement to prevent brittle modes of failure.

## 2. Material Models

The stress-strain relationship of concrete in compression is considered in view of Scott *et al.*'s model [17] due to its simplicity and robustness. The tensile capacity of concrete is assumed to drop after reaching the cracking point.

The constitutive relationship of the embedded steel bars is expressed according to the model reported by Karthik and Mander [18] that was derived in view of the general formula proposed by Ramberg and Osgood [19]. It conveniently combines the initial elastic response, yield plateau and strain hardening stages in a single rigorous form to model the actual behavior of steel reinforcement. The value of the strain hardening strain ($\varepsilon_{sh}$) is set equal to the yield strain ($\varepsilon_y$) and the strain hardening modulus ($E_{sh}$) is taken as 1% of the Young's modulus of elasticity ($E_s$).

## 3. Interfacial Shear Stress ($\tau$) and Slip ($S$) Relationship

The shear transfer mechanism is activated by the frictional resistance between the contact surfaces and the axial forces developed in the anchors crossing the interface. The former mechanism represents the concrete contribution; whereas the second case represents the influence of dowel action. The concrete contribution ($v_c$) is determined in view of Tassios and Vintzeleou [1] empirical model as a function of the lateral slip ($S$), ultimate slip value at the onset of frictional mechanism failure ($S_{cu}$) and ultimate frictional capacity of the interface ($v_{cu}$). The overall interfacial shear stress ($\tau$) corresponding to any slip ($S$) value can be obtained as the summation of concrete contribution and dowel action contribution for given material properties and interfacial

surface condition. A detailed description of this calculation procedure considering simply supported beams is provided by Alhadid and Youssef [16].

## 4. Assumptions

Assumptions considered in the current study encompasses the following:

1) Plane sections remain plane after deformation, implying that shear deformations are small relative to bending deformations.
2) Perfect bond exists between steel reinforcement and the surrounding concrete material. Thus, strain in both concrete and steel bars at the same location is identical.
3) The failure criterion of the composite beam is defined by crushing of the extreme compression fiber at a concrete ultimate strain ($\varepsilon_{cu}$) of 0.0035 [21].
4) The original RC beam and the added concrete layer are considered to deform by the same curvature through the beam length [20, 23].
5) The interfacial shear stress distribution within each region is assumed to vary as a cubic function with the distance from the zero moment section [22].

## 5. Typical Jacketed Section

The developed model is applicable to analyze symmetric continuous RC beams subjected to either uniform or concentrate loads. Fig. 1 shows the geometry and reinforcement details of a typical continuous beam that will be used for discussion throughout the chapter. The main steel reinforcement in the positive and negative moment regions are assumed to be 20% and 40% of the balanced steel reinforcement ratio, respectively. The compression steel reinforcement is 2-10M bars. The amount of jacket reinforcement is assumed as10M bars placed in one layer at the

maximum spacing provided by CSA 23.3-14 [21]. One half of the core and jacket steel bars from the hogging moment region are assumed to extend throughout the beam.

Geometry and loading scheme of the continuous beam are assumed to be symmetric about the intermediate support. Thus, one span of the beam can be modeled as a propped cantilever as shown in Fig. 2(a). This span is assumed to be composed of several members rigidly connected at their ends as illustrated in Fig. 2(b). Each segment has a defined length ($L_i$) and a distinct flexural rigidity ($EI_i$). The segment length is set at about 50 mm, which was found to enhance the accuracy based on a preliminary sensitivity analysis.

The expected trends of the moment-curvature diagrams in both the positive and negative moment regions are shown in Fig. 3. The trend for the positive moment section is characterized by three points; namely, the yielding of jacket reinforcement, yielding of the core reinforcement and crushing of concrete. The trend of the negative moment section is defined by yielding of the core reinforcement and crushing of concrete.

## 6. Proposed Calculation Algorithm

Slip, and consequently shear stress, reach their maximum value at the point of zero moment and fade away as they approach the maximum bending moment section. In continuous RC beams, each span can be divided into positive and negative moment zones as indicated in Fig. 4. To obtain the complete slip distribution along the span, the analysis procedure is carried out individually for each of the two zones. Assuming a propped cantilever model for each span, the analyzed segment within the positive moment zone is taken from the pinned support to the point of maximum bending; whereas, for the negative moment zone, this segment is taken from the point of contraflexure to the point of maximum negative bending moment at the fixed end.

The proposed analysis method comprises two main stages. In the first one, an iterative sectional analysis procedure is performed at different load levels only at the maximum sagging and hogging moment sections. This results in determining the maximum slip strain ($\Delta\varepsilon_{max}$) at these locations and the corresponding slip strain ($\Delta\varepsilon$) and slip ($S$) at the other segments along the span. In the second stage, sectional analysis is conducted directly at the remaining segments taking into account the $\Delta\varepsilon$ distribution evaluated from the first analysis step for each segment. The slip distribution is obtained while satisfying the equilibrium and compatibility conditions at each segment. Details about the mentioned steps are given below.

The primary challenges for the proposed calculation algorithm are prediction of the slip distribution along the interface and determination of the moment-curvature relationships for the beam segments shown in Fig. 2. Alhadid and Youssef [16] have proposed a calculation algorithm to determine these relationships in jacketed RC simply supported beams considering slip effect. A summary of the procedure is provided in section 6.1 showing the main changes used for analyzing continuous beams. Sectional analysis procedure to determine the equilibrium conditions is described in section 6.2. The influence of moment redistribution becomes substantial in the prediction of slip distribution along continuous beams and is discussed in section 6.3. An equivalent curvature distribution is then obtained based on the load-deflection relationship of the actual curvature distribution considering slip effect as illustrated in section 6.4.

### 6.1. Moment-Curvature at Maximum Moment Sections

For each moment zone, the average value of interfacial shear stress ($\tau_{avg}$) at any load level can be calculated assuming a direct relationship with the maximum slip strain ($\Delta\varepsilon_{max}$) located at the maximum moment section [22, 23, 24]. Therefore, the average shear stress can be given according to the expression ($\tau_{avg} = \gamma_1\, \gamma_2\, k_s\, \Delta\varepsilon_{max}\, L'$) in terms of secant interfacial stiffness, $k_s$

(N/mm$^3$); the ratios ($\gamma_1$=$\tau_{avg}/\tau_{max}$) and ($\gamma_2 = \Delta\varepsilon_{avg} / \Delta\varepsilon_{max}$); the average slip strain ($\Delta\varepsilon_{avg}$) from point of zero moment to maximum positive or negative moment; and the corresponding length, $L'$ (m).

For each of the two moment zones, the analysis procedure to determine interfacial slip distribution is carried out at each applied load level (i.e. assumed applied curvature value) until failure occurs. Firstly, initial values of the secant interfacial stiffness ($k_s$) and the shear stress distribution ratios ($\gamma_1$ $and$ $\gamma_2$) are assumed. Then, for the total curvature ($\varphi$) value of the current load increment, two equilibrium conditions are applied at the maximum moment sections: (1) equilibrium between the internal forces; and (2) equilibrium between the resultant axial forces at one side of the interface and the resultant shear force acting along the interface. Hence, the moment ($M$) and maximum slip strain ($\Delta\varepsilon_{max}$) at the maximum moment sections corresponding to the current curvature value ($\varphi$) are obtained. After that, bending moment diagram is constructed along the span assuming uniform load and considering the obtained maximum moment values. Next, the slip strain ($\Delta\varepsilon$) distribution is determined along the span with respect to the location of each segment as shown in the proposed Equation 1.

$$\Delta\varepsilon_{(i,j)} = \Delta\varepsilon_{(m,1)}\left(\frac{x_j}{L'}\right) \tag{1}$$

Where $i$ is the load step number, $j$ is the segment number and $m$ is the load step number that produces a bending moment in the mid-span segment equals to the moment applied at segment $j$. Once the slip strain ($\Delta\varepsilon$) distribution along the interface is established, both the slip ($S$) and the shear stress ($\tau$) in each segment is obtained from Equations 2 and 3, respectively.

$$S_{(i,j)} = \sum_{n=1}^{n=j}\left[\left(\Delta\varepsilon_{(i,n)}\right)\left(x_j\right)\right] \tag{2}$$

$$\tau_{(i,j)} = k_s\, S_{(i,j)} \tag{3}$$

Having obtained the slip distribution for both moment zones, continuity conditions is checked at the point of contraflexure to ensure it is satisfied by calculating the error between the obtained slip ($S$) from the sagging moment zone and the hogging moment zone. The procedure is repeated if the error is more than 1% by adjusting the slip strain ($\Delta\varepsilon$) at all segments and repeating the analysis to check equilibrium and compatibility conditions. Finally, based on the obtained slip and shear stress distributions, the secant interfacial stiffness ($k_s$) and the shear stress distribution ratios ($\gamma_1 \; and \; \gamma_2$) are calculated and compared to the initially assumed values. The analysis continues if they are equal with a tolerance of 1%, otherwise the whole procedure is repeated with the new calculated values.

If the beams are subjected to initial loading prior to jacketing, then a preliminary sectional analysis on the unjacketed sections has to be carried out first to obtain the resulting moment-curvature curve and strain profile at each beam segment. These diagrams are then included as an input in the calculation algorithm of the jacketed beam to obtain its full behavior at different loading stages before and after jacketing.

### 6.2. Sectional Analysis in Jacketed Sections

The sectional analysis procedure [25] is implemented to analyze the jacketed sections. The upper limit for the thickness of each layer is taken as 0.5 mm as it results in a better accuracy. At every loading step, an incremental curvature is applied and the strain at each strip in both the concrete core and the jacket is calculated based on its location from the centroid ($y_i$) of the jacketed section. The kinematic and compatibility conditions are considered in view of the corresponding material stress-strain relationships and Equation 4, which relates the incremental applied moment ($\Delta M$) and axial load ($\Delta P$) to the incremental curvature ($\Delta\varphi$) and axial strain ($\Delta\varepsilon_a$) by a defined stiffness matrix. In this equation, $n$ represents the number of discrete layers, $E_i$ is the elastic

modulus of layer $i$, $A_i$ is the area of layer $i$, subscript ($c$) represents concrete core and subscript ($J$) represents concrete jacket.

$$\begin{pmatrix}\Delta M\\ \Delta P\end{pmatrix}=\begin{pmatrix}\sum_{i=1}^{n}\left(E_{i,c}A_{i,c}+E_{i,J}A_{i,J}\right)y_i^2 & -\sum_{i=1}^{n}\left(E_{i,c}A_{i,c}+E_{i,J}A_{i,J}\right)y_i\\ -\sum_{i=1}^{n}\left(E_{i,c}A_{i,c}+E_{i,J}A_{i,J}\right)y_i & \sum_{i=1}^{n}\left(E_{i,c}A_{i,c}+E_{i,J}A_{i,J}\right)\end{pmatrix}\begin{pmatrix}\Delta\varphi\\ \Delta\varepsilon_a\end{pmatrix} \quad (4)$$

### 6.3. Moment Redistribution in Continuous Beams

Matrix stiffness analysis is carried out to account for moment redistribution caused by the difference in stiffness between the hogging and sagging moment zones. Fig. 5 represents an arbitrary element of the propped cantilever model subjected to external static uniformly distributed load. The distorted shape of the element can be described in terms of a translational displacement ($d_i$) and in-plane rotation ($\theta_i$) at its ends. The element stiffness is used in Equation 5 to express the joint internal forces (i.e. $P_i$ and $M_i$) as functions of the corresponding displacements (i.e. $d_i$ and $\theta_i$) and fixed-end forces due to the applied loads (i.e. $p_i$ and $m_i$) [26].

$$\begin{bmatrix}P_i-p_i\\ M_i-m_i\\ P_{i+1}-p_{i+1}\\ M_{i+1}-m_{i+1}\end{bmatrix}=(EI)_{i,j}\begin{bmatrix}\frac{12}{L_i^3} & \frac{6}{L_i^2} & \frac{-12}{L_i^3} & \frac{6}{L_i^2}\\ \frac{6}{L_i^2} & \frac{4}{L_i} & \frac{-6}{L_i^2} & \frac{2}{L_i}\\ \frac{-12}{L_i^3} & \frac{-6}{L_i^2} & \frac{12}{L_i^3} & \frac{-6}{L_i^2}\\ \frac{6}{L_i^2} & \frac{2}{L_i} & \frac{-6}{L_i^2} & \frac{4}{L_i}\end{bmatrix}\begin{bmatrix}d_i\\ \theta_i\\ d_{i+1}\\ \theta_{i+1}\end{bmatrix} \quad (5)$$

The proposed method modifies the matrix analysis procedure by incorporating the influence of slip. The $M$-$\varphi$ diagram for each section is first calculated while accounting for slip as explained in section 6.1. The secant stiffness is then evaluated for a given moment. For each loading step, the relationship in Equation 14 is carried out for each segment ($i$) considering the secant flexural stiffness ($j$) obtained from the corresponding $M$-$\varphi$ diagram at the specified load level. The equilibrium and compatibility conditions obtained from the matrix structural analysis

and the slip calculation algorithm must be verified simultaneously. Hence, nested iterations are required for each load step to satisfy equilibrium and continuity for each segment along the beam. The moment redistribution along the beam is dictated by the flexural stiffness ratio between the hogging and sagging moment regions [27]. Fig. 3 shows the $M$-$\varphi$ relationships for the positive and negative moment sections of an arbitrary continuous beam. Because of the higher initial stiffness of the negative moment section, the point of zero moment is shifted away from the intermediate support towards the mid-span. A sketch of the bending moment diagram and the flexural rigidities within the elastic loading stage for both the hogging and sagging regions are illustrated in Fig. 4(b). In this case, the flexural rigidity is constant within each region but vary between the positive and negative zones. Bending moment diagram is obtained based on the stiffness distribution along the span.

Once the negative moment section yields, its secant stiffness will decrease gradually with the applied load until it equates the stiffness at the positive moment section. In this case, the bending moment diagram obtained from stiffness analysis will be identical to that obtained from elastic structural analysis. As the load keeps increasing, the hogging-to-sagging stiffness ratio further decreases resulting in a shift of the point of zero moment towards the intermediate support as more proportion of the additional load is carried by the sagging moment region. However, since the length of each element, and consequently the reinforcement, is assumed to be fixed up to failure, part of the assumed hogging moment region will start to resist small amount of positive moment as shown in Fig. 4(c). The influence of this overlap is insignificant since the moment values adjacent to the point of contraflexure are relatively low. Failure of the beam is activated by crushing of the extreme concrete fibers at the intermediate support where the maximum moment is anticipated. The expected load-deflection curve of the modeled propped cantilever is presented

in Fig. 4(d). It shows both the point of maximum deflection and the inflection point that is determined at the initial loading steps and fixed throughout the analysis.

### 6.4. Load-Deflection Relationship and Equivalent Curvature Distribution

Once the slip effect is incorporated in a unique $M$-$\varphi$ diagram for each segment, the area-moment method is carried out to determine the deflection at distance of 0.4215 of the span away from the edge support. This distance defines the location of maximum deflection for symmetric typical continuous beam supporting a uniformly distributed load [27].

Having obtained the load-deflection curve of the jacketed beam including slip effect, the actual curvature distribution of the propped cantilever is determined at different loading steps for each segment. These values are obtained from the corresponding $M$-$\varphi$ diagram taking into account the partial composite action according to the jacketing scheme used. After that, positive ($\varphi^{+}_{eq}$) and negative ($\varphi^{-}_{eq}$) equivalent curvatures are obtained by assuming that the curvature distribution along the beam is similar to the monolithic behavior of jacketed beams. Therefore, at each loading value, and consequently deflection, equivalent maximum positive and negative curvatures corresponding to the applied moment can be obtained. Hence, an equivalent $M$-$\varphi$ curve can be obtained for the jacketed beam taking into consideration slip effect. The load-deflection curve can be determined at any point using the moment-area theorem and the anticipated deflection shape.

## 7. Validation

The capability of the proposed model to capture the flexural behavior of simply supported jacketed RC beams was previously validated [16]. For continuous jacketed beams, the experimental program performed by Cheong and MacAlevey [15] is considered. Fig. 6 shows the longitudinal and cross-sectional views of the jacketed continuous beam. Initially, the T-section

concrete core was cast according to the cross-sectional dimensions and reinforcement distribution shown. After 28 days of curing, the contact surfaces were roughened prior to applying the jacket. The concrete compressive strength was reported as 30 MPa for the core and 60 MPa for the jacketing material. The tensile yield strength of bar size $\Phi$16, $\Phi$25, $\Phi$6, $\Phi$10 and $\Phi$8 were 583 MPa, 567 MPa, 290 MPa, 321 MPa and 407 MPa, respectively. The tensile ultimate strength for the same sequence of bars were 652 MPa, 670 MPa, 394 MPa, 424 MPa and 477 MPa, respectively. The jacketed beam was subjected to two-point loading scheme at one span only as shown in Fig. 6(a).

The proposed calculation method is carried out to determine the flexural behavior of the jacketed continuous beam in terms of the load-deflection curve at the center of the loaded span. The load-deflection curves assuming monolithic and partially composite behaviors are then plotted and compared with the ones obtained experimentally by Cheong and MacAlevey [15]. Fig. 7 shows that the percent errors in initial stiffness between the experimental results and the proposed analytical ones are 7.9% and 2.9% assuming both monolithic and partial interaction, respectively.

Cheong and MacAlevey [15] reported that a slip between the concrete core and the surrounding jacket was detected without presenting any more data about the slip distribution along the interface. The relatively close variations in the flexural stiffness in the elastic range indicates that the proposed model is capable of predicting the load-deflection behavior prior to steel yielding. Introducing the slip effect in the analysis further improves the predictions by lowering the stiffness to approach the experimental trend. The value of friction coefficient chosen in the analysis is 0.8 to account for surface treatment using electric chisel used in the experiment (i.e. roughened surface) [28]. Regarding the ultimate load, the percent error between the experimental and proposed analytical results is 6.2% and 3.8% by ignoring and including the slip effect, respectively.

Cheong and MacAlevey [15] reported that the observed failure is brittle caused by the excessive tensile stresses at the narrow bearing supports, which was not accounted for in the proposed model.

Due to the lack of experimental results, a finite element model is developed assuming monolithic behavior using ANSYS Software for further validation. The connection between the concrete core and the surrounding jacket is modeled assuming full bond between the adjacent nodes. Geometrical details of both the concrete core and the jacket are modeled using SOLID65, which is an 8–node solid element. This element is capable of cracking under tensile stresses and crushing when subjected to excessive compressive stresses. The element is defined by 8 nodes each having three translational degrees of freedom. The steel main and secondary steel bars in both the core and the jacket are modeled using LINK180 element. This element is a uniaxial tension-compression element with three degrees of freedom at each node corresponding to the X, Y and Z coordinates. The supporting plates used at the location of applied concentrated loads or at the supports are modeled using SOLID185 element assuming elastic behavior. This element is also defined by 8 nodes each having 3 translational degrees of freedom in each direction. A sensitivity analysis is performed to determine the optimum mesh size as shown in Fig. 8. The stiffness and yield stress obtained from the finite element model are 8.7% and 10.2% higher than the corresponding experimental values as shown in Fig. 7, respectively. This variation is attributed to neglecting the influence of slip between the concrete core and the attached jacket. Fig. 7 also shows that the load-deflection curve obtained from the proposed analytical model assuming monolithic action follows the same trend as that obtained from the developed finite element model with a percent difference of 5.2% and 6.4% for stiffness and yield stress, respectively.

## 8. Parametric Study

A parametric study is carried out to investigate the influence of different design parameters on the performance of jacketed continuous RC beams. The concrete compressive strength is taken as 25 MPa, 30 MPa and 35 MPa; and the steel yield strength is taken as 300 MPa, 400 MPa and 500 MPa. For each of the analyzed sections, the mechanical properties are assumed to be the same for the concrete core and its jacket. The coefficient of friction ranges according to ACI [28] between 0.4 for smooth concrete surface to 1.4 for intentionally highly roughened concrete in increments of 0.2. The beam's cross-sectional dimensions are defined with reference to the existing beam height (300 mm, 450 mm and 600 mm), jacket thickness (100 mm, 150 mm and 200 mm), existing beam width (200 mm, 300 mm and 400 mm), and beam span (3 m, 4 m and 5 m). The steel reinforcement distribution along the beam is shown in Fig. 1 in which the balanced steel reinforcement ratio is determined with regard to CSA A23.3 [21]. Jacketing from one side at the soffit of all beams is adopted in the analysis. Each section is analyzed 63 times to account for the considered variables. Therefore, a total of 5103 different cases are considered in the current parametric study.

## 9. Moment-Curvature Behavior

The following discussion refers to the beam sections whose geometrical and mechanical properties are listed in Table 1. These sections are considered to examine the influence of slip on flexural behavior of jacketed RC beams due to the variation of jacket thickness, beam width, beam height, span, concrete compressive strength and steel grade. Figs. 9 and 10 show the initial stiffness values for each section assuming full and partial composite actions (assuming a friction coefficient of 0.4) under both sagging and hogging moments, respectively. The reduction in initial stiffness

caused by slip is indicated as a percentage in the corresponding figures. Fig. 11 describes the variation of the reduction rate in stiffness (as percentage) due the variation of each of the aforementioned parameters. Reference to Table 1 and Figs. 9, 10 and 11 is made throughout the following discussion.

### 9.1. Effect of Jacket Thickness ($h_J$)

Beams B-1, B-2 and B-3 are considered for comparison. Figs. 12 and 13 illustrate the influence of varying the jacket thickness on the flexural behavior of continuous beams in view of the $M$-$\varphi$ relationships along the sagging and hogging moment regions, respectively. The flexural behavior in the sagging moment region is characterized by yielding of jacket reinforcement ensued by yielding of core reinforcement and a yielding plateau until failure by concrete crushing. Regarding the hogging moment region, the yielding plateau occurs immediately after yielding of the tension steel bars located in the original beam. The same behavior is found for the remaining parameters; therefore, only the stiffness values are included in the discussion.

The stiffness reduction rate in both the sagging and hogging moment zones slightly decreases with increasing the jacket thickness. The ductility increase is insignificant when slip is considered for the sagging moment region indicating that the compressive strains at the extreme compression fibers reach the concrete crushing strain value at the same curvature. This happens since the axial stress in the jacketing layer assuming both monolithic and partially composite actions become identical beyond the yielding point of the jacket steel bars regardless of the slip strain. However, in the hogging moment region, as the jacket thickness increases, the contribution of the concrete material and the compression steel bars located in the jacket layer becomes more prevalent relative to the entire section. Therefore, slip strain reduces the generated compressive stresses within the jacket layer at the same curvature value. This results in delaying the concrete crushing and

consequently increasing the ductility as the jacket height increases relative to the monolithic beams.

### 9.2. Effect of Beam Width ($b_c$)

Increasing the beam width results in a consequent increase in both the initial stiffness and capacity with minor influence on the flexural ductility. Regarding the slip influence, increasing the beam width results in decreasing the reduction rate of the initial stiffness in both sections. This is justified by the larger contact area between the concrete core and the jacket that is provided by the additional beam width. Two main differences arise from changing the location of the contact surface with respect to the neutral axis. When the interface is located at the tension side (i.e. sagging moment section), the reduction in the elastic stiffness is relatively smaller than the case of hogging moment. This variation in stiffness reduction is attributed to the contribution of both concrete and steel in determining the slip strain ($\Delta\varepsilon$) at each section. For the sagging moment region, the bending stresses at the tension side are resisted by both the core steel bars and the jacket steel bars especially after concrete cracking takes place. This means that the steel in the jacketing layer sustains part of the generated tensile stresses and the remaining part is resisted by the steel bars in the original beam. Thus, the slip strain required to achieve equilibrium at any section along the jacketed beam is governed by a portion of the total tensile stress generated at a given applied load. A different situation is observed along the hogging moment region where the jacketing layer is at the compression side. In this case, the entire concrete material is utilized along with the jacket steel bars to resist the same applied load. This indicates that a larger portion of bending is carried by the jacket part causing an increase in the slip strain required to achieve equilibrium at any segment along the hogging moment region.

The other difference that prevails from changing the location of the interface with respect to the neutral axis is the point which the $M$-$\varphi$ curves ignoring and including slip effects follow the same path. For the sagging moment region, the major difference in the moment-curvature diagram is within the elastic region before yielding of the jacket steel bars. This is justified by knowing that the axial force at any section is determined by the jacket steel bars. So, once these bars yield, the tensile forces in the jacket steel bars becomes almost constant and any increase depends on the strain hardening modulus. Thus, after jacket yielding is reached, the influence of slip strain becomes negligible in changing the behavior of the $M$-$\varphi$ diagram compared to its monolithic counterpart. Regarding the hogging moment region, yielding point is dictated by the tensile steel reinforcement in the concrete core. Therefore, the yielding point considering slip occurs at a larger curvature value compared to the monolithic case. Since the tensile stresses in the jacketing layer are governed by the compression behavior of both the concrete material and the embedded jacket steel bars, the influence of slip strain remains considerable in reducing the moment carrying capacity at a given curvature. As the load increases, the effect of slip strain diminishes until the moment-curvature behavior of the partially composite section becomes identical to the monolithic one.

### 9.3. Effect of Existing Beam Depth ($h_c$)

In both the sagging and hogging moment cases, increasing the existing section height increases both the elastic stiffness and capacity of the jacketed beams. This is justified by the larger concrete material available in the compression side and the longer lever arm the tension steel bars have. The ductility, on the other hand, decreases as the section height increases and becomes even more pronounced if the interface is at the compression side. This drop in ductility is related to the higher stresses developed in the tension steel bars as the original beam height rises at any curvature

level. Therefore, at the same applied bending moment, this higher stress at the tension steel bars is translated into higher compressive stresses at the compression face of the jacketed beam causing the concrete to reach its crushing strain at lower curvature values. Regarding the slip influence on the flexural behavior of these beams, the initial stiffness reduction rate decreases as the original section height increases for both the sagging and hogging moment cases. This decrease is a result of the higher slip strain required to equilibrate the axial force within the jacket with the horizontal shear force along the interface.

### 9.4. Effect of Beam Span (*L*)

The *M*-$\varphi$ curve assuming monolithic interaction between the core and the jacket are identical regardless of the span as they depend merely on the cross-sectional properties. However, including the slip effect activates the partially composite action and consequently the horizontal shear distribution along the interface becomes a major player in determining the flexural behavior of any section along the beam. In both the sagging and hogging moment cases, as the span increases, the elastic stiffness reduction rate decreases proportionally. This observation is justified by the higher contact area provided by the larger span and consequently the increased frictional forces along the jacketed beam. For the positive moment section, the partially composite flexural behavior becomes identical to the monolithic counterpart once jacket steel bars yield. This happens due to the small variation in the axial stresses governed by the strain hardening modulus of jacket steel bars after yielding occurs. Thus, at the same curvature value, the stress in these steel bars is almost identical to the ones in the monolithic case. Although it still exists, the influence of slip strain diminishes even more at higher loading values due to the higher contribution of compression concrete and tension core steel bars while the stresses in the jacket steel bars remain almost constant. Regarding the hogging moment region, the variation between the partially composite scenario and monolithic

behaviors persists within a portion of the inelastic region. This occurs since the jacketing layer is governed by the compressive stresses developed in concrete and the embedded steel bars rather than the tensile stresses generated merely in the steel bars. Thus, even after yielding of the section takes place, the axial force within the jacket at any section remains different from the monolithic case due to the influence of slip strain which decreases the jacket stresses at any curvature value. At higher loading values, the slip strain becomes less pronounced relative to the higher curvature values and consequently its influence becomes less substantial.

### 9.5. Effect of Concrete Compressive Strength ($f'_c$)

Increasing the concrete compressive strength results in a consequent increase in the beam capacity as it resists higher stresses for the same peak strain value. Also, increasing the concrete grade rises the concrete modulus resulting in a higher elastic stiffness value. Regarding the slip effect, increasing the concrete compressive strength decreases the stiffness reduction rate indirectly through increasing the friction between the two surfaces. This is inferred by examining the change in flexural behavior when slip is considered in both the sagging and hogging moment regions.

### 9.6. Effect of Steel Grade ($f_y$)

Increasing the steel yield strength has a negligible influence on the initial stiffness of the jacketed beams but a substantial enhancement to its capacity. The main reduction in stiffness will be in the elastic zone in which the steel elastic modulus plays the major role. Considering slip in the analysis shows that as the steel grade increases, the drop in flexural stiffness also increases for both the sagging and hogging moment sections. This happens since the steel bars with higher grade within the jacket resist larger axial forces before yielding and consequently result in higher shear

stresses to achieve equilibrium. These higher stresses result in larger slip and consequently larger slip strain that reduces the flexural stiffness of the jacketed beams.

## 10. Interfacial Slip Behavior

The influence of interfacial slip between the concrete core and the underlying jacket layer is investigated in view of the slip strain ($\Delta\varepsilon$), slip ($S$) and interfacial shear stress ($\tau$) distribution along the continuous beams under different loading values. Beam B-14 in Table 1 is considered for the following discussion. The coefficient of friction between the two surfaces is taken as 0.4 and 1.0 which represent untreated surfaces and intentionally roughened surfaces, respectively. Figs. 14 through 18 represent the distribution along one span only of the continuous beam.

### 10.1. Slip Strain ($\Delta\varepsilon$) Distribution

Figs. 14 and 15 illustrate the slip strain distribution from the edge support towards the intermediate support for coefficient of friction of 0.4 and 1.0, respectively. Four loading values representing the elastic range, onset of jacket yielding, onset of core yielding and maximum capacity of the section at the intermediate support at the onset of concrete crushing. Both figures show the same trend in which the slip strain at any section increases with the applied load except at the points of zero moment (i.e. the edge support and the point of contraflexure). This increase corresponds to the rise in the axial stresses within the jacket layer to maintain the equilibrium condition with the interfacial shear along the contact plane.

The maximum slip strain reaches the peak value at two points corresponding to the maximum positive bending moment and the maximum negative bending moment sections. The slip strain is always higher at the intermediate support than the maximum positive moment for two main reasons. The first one is that the sagging moment region extends along a larger distance than the

hogging moment zone resulting in a larger contact area and friction resistance and consequently less slip strain in the former case. Also, the slip strain is proportional to the bending moment that develop axial stresses within the jacket. Since the negative moment at the middle support is always larger than the maximum positive moment at any loading value, the slip strain follows the same trend and becomes higher at the intermediate support. By comparing the curves in Fig. 14 for $\mu$ = 0.4 to their counterparts in Fig. 15 for $\mu$ = 1.0, higher slip strain values at any given load are observed in the former case. This difference occurs due to the lower interfacial stiffness as the friction coefficient decreases. Thus, for the same axial stresses in the jacket, higher slip strain is required to achieve equilibrium with the interfacial shear stress. By roughening the concrete surface prior to jacketing, the slip strain at the maximum positive moment section drops from about 0.39 to 0.16 indicating a ratio of 58.9%. This drop at the maximum negative moment section is shown to be from 1.25 to 0.66 with a ratio of 47.2%. The slip strain increasing rate rises at higher loading values compared to the elastic region in both the hogging and sagging moment regions. For the maximum positive moment section, increasing the uniformly applied load from 30 kN/m to 90 kN/m along the beam results in a consequent increase of the slip strain by just $0.07\times10^{-3}$ for the untreated surface and by just $0.03\times10^{-3}$ for the roughened surface. After yielding occurs, increasing the load by about 10 kN/m results in an increase of $0.16\times10^{-3}$ and $0.08\times10^{-3}$ for the smooth and rough surfaces, respectively. The same observation applies for the maximum negative moment section but with different increasing rate. This is explained by the larger curvature the beam undergoes within the yielding plateau corresponding to any variation in the applied load relative to the elastic range.

### 10.2. Slip (S) Distribution

The slip distribution along the interface considering both smooth and rough surfaces are shown in Figs. 16 and 17, respectively. As shown in these figures, the maximum slip values are obtained at the edge support and the point of contraflexure that both correspond to the sections of zero moments. On the contrary, relative slip between the two surfaces becomes negligible at the locations of maximum positive and negative moments. The same figures also show that slip values at sections closer to the edge support are slightly less than those near the middle support. This reduction is due to concrete cracking in the sagging moment region that takes place during the initial loading stage. When the concrete jacket is cracked, only the jacket reinforcement contributes in resisting the generated axial force resulting in lower level of shear stresses transferred along the interface.

In the hogging moment region, both concrete and the jacket steel bars are active and resist the bending moment in terms of compressive stresses. This results in larger contribution of the jacket and consequently higher shear stress to be transferred along the interface as translated by the higher slip values. The slip increasing rate after the first yielding point is higher than the rate before yielding for both kinds of surface treatment. For example, increasing the applied load within the elastic region from 30 kN/m to 90 kN/m results in a consequent increase in the maximum slip at the edge support from 0.04 mm to just over 0.12 mm for the untreated surface case. However, after the yielding point is reached, increasing the load by just 10 kN/m results in extra relative sliding between the two surfaces of about 0.18 mm. The same observations are shown for the roughened surface case. This higher rate of slip rise is justified by the higher curvature the beam exhibits after reaching the yielding point for the same amount of load compared to the elastic range. Consequently, the slip strain ($\Delta\varepsilon$) at the yielded segments increases resulting in a larger

increase in slip. By examining both figures, the slip values considering smooth surfaces are higher than the ones obtained assuming roughened surfaces at any section for the same loading level. For example, the slip at the edge support for the former case is 138.9% higher than the second case at the ultimate loading value. This is justified by the higher frictional resistance and consequently the higher interfacial stiffness as the original beam surface is roughened. It is worth mentioning that at the ultimate load, the slip value at any section is less than the failure value defined in the slip model of about 2 mm.

### 10.3. Interfacial Shear Stress ($\tau$) Distribution

Figs. 18 and 19 detail the horizontal shear stress distribution along the interface between the concrete core and the attached jacket layer considering untreated and roughened surfaces, respectively. As shown in both figures, the distribution follows a third order parabolic function as initially assumed. The shear values are then determined by carrying out both sectional and longitudinal analyses to satisfy the equilibrium, compatibility and constitutive conditions. Also, the figures demonstrate the direct relationship that relate the interfacial shear stress ($\tau$) to the slip ($S$) at any section through the interfacial stiffness ($k_s$). Since the shear-slip model at the interface is non-linear, the secant interfacial stiffness varies depending on the slip value. For the smooth connection, the interfacial shear to slip ratio at the edge support is obtained as 3.4 N/mm$^3$ for all distributions up to the yield point and 2.9 N/mm$^3$ at ultimate. The same conclusion is drawn by comparing the curves in the second figure but with the secant interfacial stiffness of 9.1 N/mm$^3$ up to the yield point and 7.7 N/mm$^3$ at ultimate at the same section. As expected, the interfacial stiffness at any given load is higher when the original beam surface is roughened compared to the untreated case. Although the slip distribution along the interface is different for both cases, the interfacial shear stress distribution is almost identical. This is justified by the variation of the

interfacial stiffness between both cases that result in equilibrium between the axial force in the jacketing layer and the horizontal shear force at any segment along the interface. The same observations are shown in the hogging moment region.

## 11. Proposed Expressions for the Effective Stiffness

Having developed and verified an analytical procedure to analyze jacketed continuous RC beams considering the influence of interfacial slip, a parametric study including 5103 specimens is carried out to determine the contribution of various parameters on the flexural behavior of such beams. These parameters encompass the beams' geometrical properties, mechanical properties and interfacial behavior between the core and the RC jacket. The outcomes show that ignoring the relative slip between the two substrates may overestimate the flexural stiffness causing serviceability issues such as larger deflections and unexpected cracking. Therefore, the influence of slip should be considered when designing such jacketed beams. Including the influence of slip in the analysis is tedious and requires a sequence of nested iterations that may not be convenient for design engineers. Here comes the importance of providing the engineers with expressions that improves the accuracy of their designs with less time and effort. The extent of flexural stiffness reduction as well as the point at which both the monolithic and partially composite curves becomes almost identical differ between the sagging and hogging moment regions. Therefore, different expressions are provided to adjust the monolithic $M$-$\varphi$ diagram of each region by considering the slip effect. Equations 6 through 9 provide the expressions for $\alpha_y$ and $\alpha_u$ that represent the yield monolithic factor and ultimate monolithic factor for the hogging moment section, respectively. Equations 10 and 11 presents the yield monolithic factor ($\alpha_y$) for the sagging moment section.

$$\alpha_y^{-ve} = \left(\xi_y^{-ve}\right) + \left[22.6645\left(\xi_y^{-ve}\right)^2 - 46.3178\left(\xi_y^{-ve}\right) + 23.6573\right] \quad (6)$$

$$\begin{aligned}\xi_y^{-ve} = {} & 1.15545 - 2.661\times10^{-4} f_c' + 3.229\times10^{-5} f_y - 1.266\times10^{-5} L \\ & + 3.30\times10^{-7} b_c^2 - 2.811\times10^{-4} b_c - 1.704\times10^{-5} h_c \\ & + 5.22\times10^{-6}\frac{h_J^2}{b_c} - 1.57\times10^{-5} h_J - 0.037306\,\mu \geq 1.0\end{aligned} \quad (7)$$

$$\alpha_u^{-ve} = \left(\xi_u^{-ve}\right) + \left[1.4756\exp\left(138.9291\,\xi_u^{-ve}\right)\right] \quad (8)$$

$$\begin{aligned}\xi_u^{-ve} = {} & 1.11070 - 1.108\times10^{-4} f_c' + 3.459\times10^{-5} f_y - 1.018\times10^{-5} L \\ & + 1.90\times10^{-7} b_c^2 - 1.784\times10^{-4} b_c - 8.39\times10^{-6} h_c \\ & + 2.857\times10^{-5}\frac{h_J^2}{b_c} - 9.06\times10^{-6} h_J - 0.033465\,\mu \geq 1.0\end{aligned} \quad (9)$$

$$\alpha_y^{+ve} = \left(\xi_y^{+ve}\right) + \left[20.3463\left(\xi_y^{+ve}\right)^2 - 41.0203\left(\xi_y^{+ve}\right) + 20.6732\right] \quad (10)$$

$$\begin{aligned}\xi_y^{+ve} = {} & 1.11354 - 1.108\times10^{-4} f_c' + 3.459\times10^{-5} f_y - 1.018\times10^{-5} L \\ & + 2.20\times10^{-7} b_c^2 - 2.043\times10^{-4} b_c - 8.39\times10^{-6} h_c \\ & - 2.190\times10^{-5} h_J - 0.033465\,\mu \geq 1.0\end{aligned} \quad (11)$$

Where $f_c'$ is the concrete compressive strength in MPa; $f_y$ is the steel yield strength in MPa; $L$ is the beam span in mm; $b_c$ is the section width in mm; $h_c$ is the section height in mm; $h_J$ is the jacket thickness in mm and $\mu$ is the coefficient of friction between the original beam and the attached jacket. If the beams were subjected to initial loading before jacketing, then the monolithic factors should be reduced according to the expressions given in Equations 12, 13 and 14 for hogging ultimate monolithic factor, hogging yield monolithic factor and sagging yield monolithic factor, respectively.

$$\left(\alpha_y^{-ve}\right)_{initial} = \alpha_y^{-ve} - \left(\frac{M_{initial}}{M_{u,unjacketed}}\right)^{1.327}\left(\alpha_y^{-ve} - 1.0\right) \geq 1.0 \quad (12)$$

$$(\alpha_u^{-ve})_{initial} = \alpha_u^{-ve} - \left(\frac{M_{initial}}{M_{u,unjacketed}}\right)^{0.849} (\alpha_u^{-ve} - 1.0) \geq 1.0 \quad (13)$$

$$\left(\alpha_y^{+ve}\right)_{initial} = \alpha_y^{+ve} - \left(\frac{M_{initial}}{M_{u,unjacketed}}\right)^{1.113} \left(\alpha_y^{+ve} - 1.0\right) \geq 1.0 \quad (14)$$

Where $M_{initial}$ is the maximum applied moment during jacketing and $M_{u,unjacketed}$ is the flexural capacity of the unjacketed section. In these expressions, the section subjected to maximum negative moment is considered to determine the hogging moment, while the section subjected to maximum positive moment is used in evaluating the sagging moment. Figs. 20 (a) and 20(b) detail the variation in a typical equivalent moment-curvature diagrams assuming monolithic and partially composite sections without and with initially applied load, respectively.

The main parameters defining the curves in Fig. 20 are the yield moment ($M_y$) and the corresponding equivalent curvature assuming monolithic ($\varphi_y$) and partially composite ($\varphi^*_y$) actions; and ultimate moment ($M_u$) and the corresponding equivalent curvature assuming monolithic ($\varphi_u$) and partially composite ($\varphi^*_u$) actions. For the initially loaded beams, two additional terms are introduced that define the both the moment ($M_{initial}$) and the equivalent curvature ($\varphi_{initial}$) corresponding to the initial loading value at the onset of jacketing as indicated in Fig. 20(b).

The proposed design procedure is summarized in the following three steps to obtain the actual load-deflection curve considering the sliding between the two surfaces:

1) Plot the $M$-$\varphi$ diagram for the sections representing both the sagging and hogging moment regions assuming monolithic interaction between the original beam and the attached jacket. The hogging $M$-$\varphi$ diagram is assumed bilinear and can be plotted by evaluating the yield and ultimate points. Regarding the sagging moment section, only the yield point is required since concrete crushing usually occurs at the negative moment section in continuous beams subjected to static loads.

2) Modify these *M*-$\varphi$ diagrams in view of Fig. 10(a) and Equations 6 through 11 for beams not subjected to initial load during jacketing. If the beam was subjected to initial loading prior to jacketing, then modify the *M*-$\varphi$ diagrams in view of Fig. 20(b) and Equations 12 through 14 taking into account the initial applied load level and the monolithic factors for unloaded beams obtained from Equations 6 through 11.
3) Use the equivalent *M*-$\varphi$ diagrams obtained at the sagging and hogging moment regions along with the moment-area theorem to obtain the load-deflection diagram at any point along the beam.

The expectation function of the proposed monolithic factors is determined considering nonlinear regression analysis of the data. Figs. 21(a), 21(b) and 21(c) present the line of equality corresponding to $\alpha_y^{-ve}$, $\alpha_u^{-ve}$ and $\alpha_y^{+v}$ without initial loading, respectively.

The line of equality plots for all factors reveal that the model provides a very good prediction of the actual behavior. Residual analysis for the three factors clearly shows a normally distributed pattern of the residuals about the mean. The small positive value of mean indicates that the proposed expressions tend to slightly round up the actual factor resulting in higher stiffness reduction and therefore more conservative estimates. Similar statistical analysis is carried out for the factors when initial load level is considered and a very good agreement is also found.

## 12. Summary and Conclusions

An investigation of the influence of RC jackets on the flexural behavior of continuous RC beams was presented. A parametric study including 5103 symmetric continuous beams subjected to uniformly distributed loads is carried out. The jacket is applied from one side at the soffit of all beams. Different parameters including the geometrical properties (i.e. original beam width,

original beam depth, jacket thickness and beam span); mechanical properties (i.e. concrete compressive strength and steel yield strength); and surface treatment (i.e. interfacial friction coefficient) are investigated. An analytical model encompassing sectional and interfacial analyses were developed taking into account that constitutive, compatibility and equilibrium conditions are satisfied. The accuracy of the proposed model was validated in view of relevant experimental results found in literature. The parametric study revealed that including the slip influence in the analysis results in a reduction of stiffness that should be considered when designing jacketed sections. For the beams considered in the analysis, ductile failure mode characterized by yielding of tension steel bars followed by concrete crushing at the extreme compression fiber was detected. The effect of each of the studied parameters on the $M$-$\varphi$ relationship is similar for both the hogging and sagging moment regions but shown to be more pronounced in the former zone. A design procedure and stiffness monolithic factors are introduced in terms of the studied parameters to obtain the flexural behavior of the continuous RC beams.

**Table 1: Geometry of the discussed jacketed beams**

| Section | Studied Parameters | Span (m) | $b_c$ (mm) | $h_c$ (mm) | $h_J$ (mm) | $f_c^{'}$ (MPa) | $f_y$ (MPa) |
|---|---|---|---|---|---|---|---|
| B-1 | $h_J, f_c^{'}, f_y$ | 3 | 200 | 300 | 100 | 30 | 400 |
| B-2 | $h_J$ | 3 | 200 | 300 | 150 | 30 | 400 |
| B-3 | $h_J$, $b_c$, $h_c$, Span | 3 | 200 | 300 | 200 | 30 | 400 |
| B-4 | $h_c$ | 3 | 200 | 450 | 200 | 30 | 400 |
| B-5 | $h_c$ | 3 | 200 | 600 | 200 | 30 | 400 |
| B-6 | $b_c$ | 3 | 300 | 300 | 200 | 30 | 400 |
| B-7 | $b_c$ | 3 | 400 | 300 | 200 | 30 | 400 |
| B-8 | Span | 4 | 200 | 300 | 200 | 30 | 400 |
| B-9 | Span | 5 | 200 | 300 | 200 | 30 | 400 |
| B-10 | $f_c^{'}$ | 3 | 200 | 300 | 100 | 25 | 400 |
| B-11 | $f_c^{'}$ | 3 | 200 | 300 | 100 | 35 | 400 |
| B-12 | $f_y$ | 3 | 200 | 300 | 100 | 30 | 300 |
| B-13 | $f_y$ | 3 | 200 | 300 | 100 | 30 | 500 |
| B-14 | $\Delta\varepsilon$, $S$, $\tau$ | 3 | 200 | 450 | 150 | 30 | 300 |

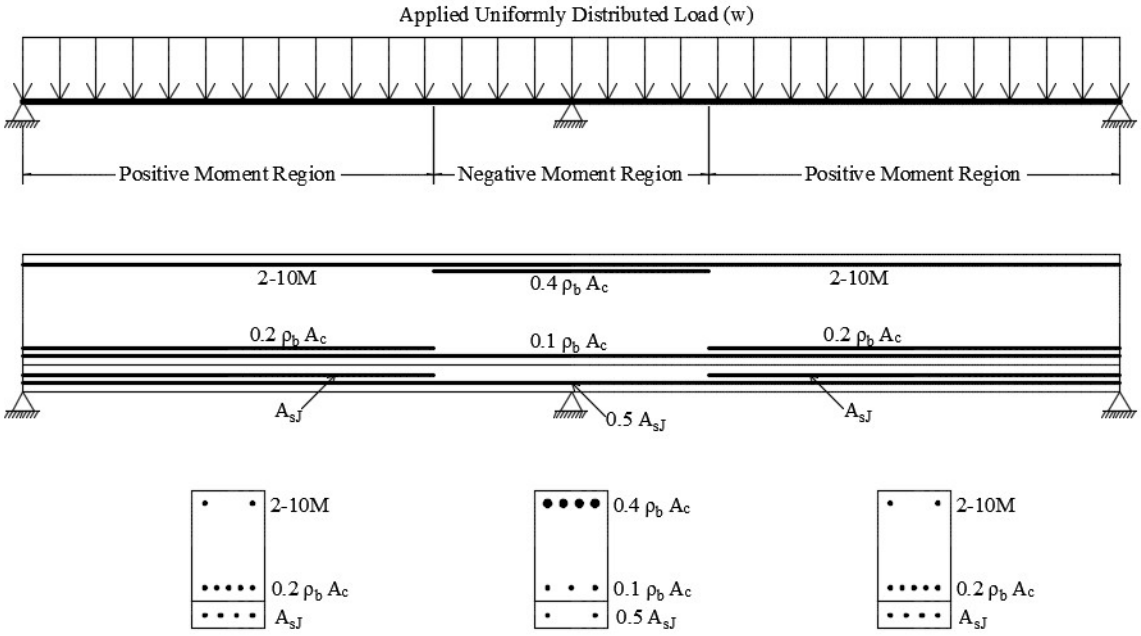


**Figure 1: Continuous beam loading scheme and reinforcement configuration**

(a) Actual beam

(b) Structure coordinate numbers

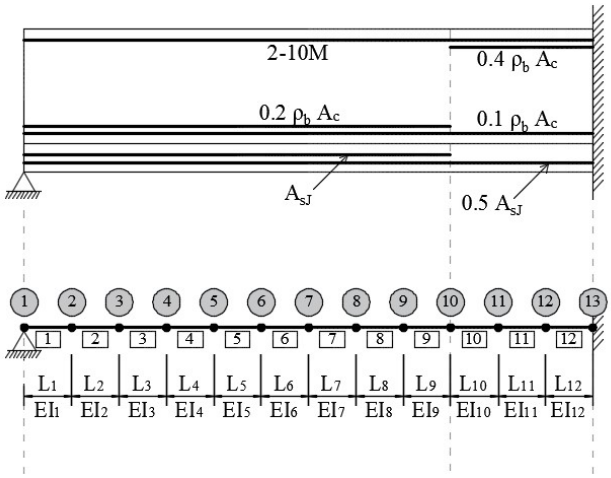


**Figure 2: Propped cantilever analytical model**

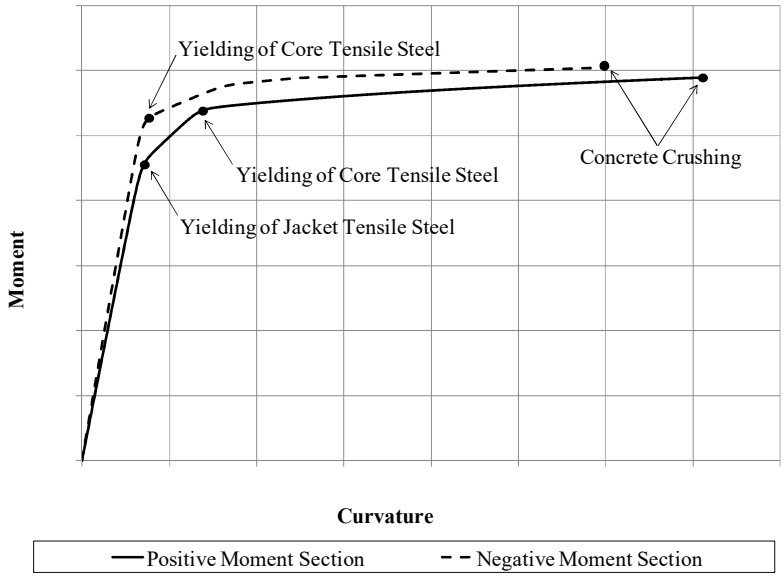


**Figure 3: Moment-curvature diagrams for positive and negative moment sections**

**(a) propped cantilever idealization**

**(b) bending moment diagram showing the point of zero moment**

**(c) bending moment diagram showing the point of zero moment**

**(d) anticipated deflection shape of the propped cantilever**

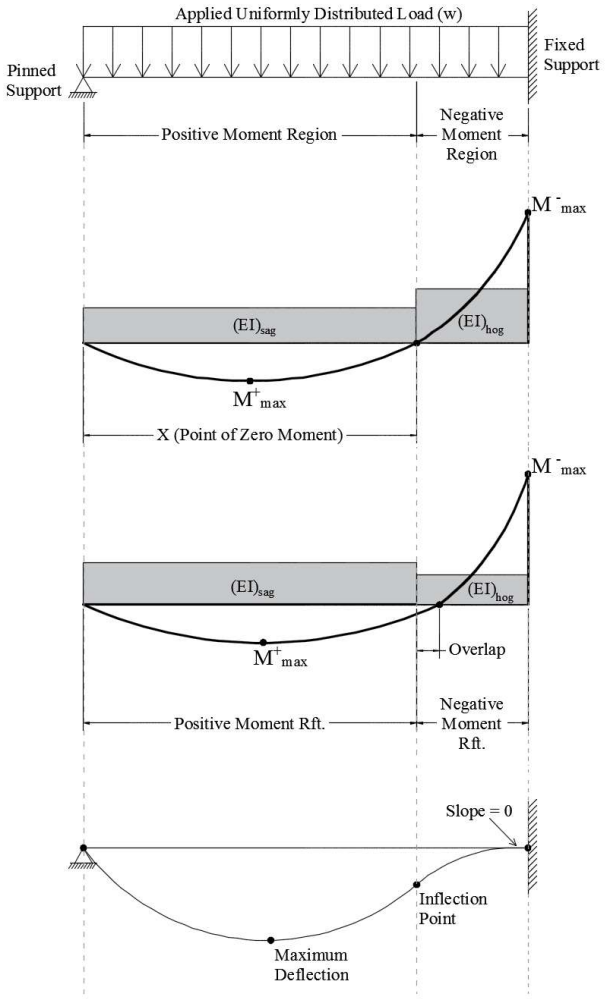


**Figure 4: Bending moment and deflection profile of the propped cantilever model**

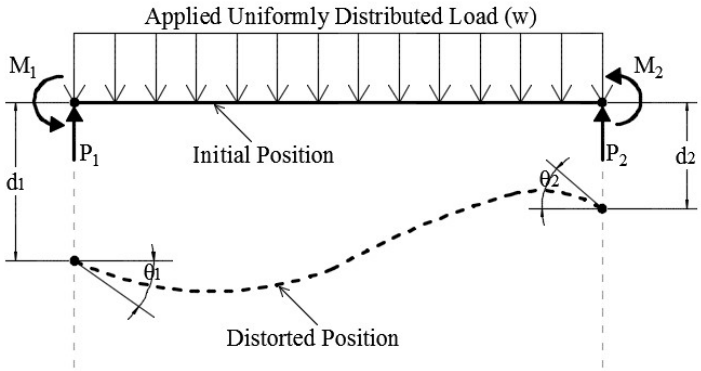


**Figure 5: Element forces and displacements**


Note: Stirrups are ϕ6 spaced at 115 mm along the beam

**(a) jacketed beam longitudinal view and location of the applied loads**

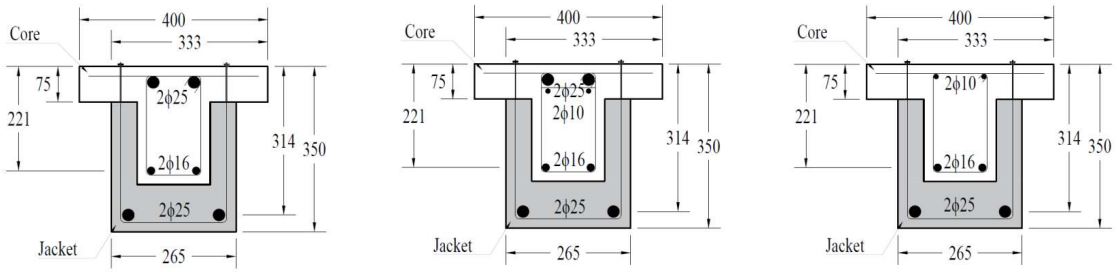


**Sec A-A** **Sec B-B** **Sec C-C**

**(b) cross-sectional views.**

**Figure 6: Longitudinal and cross-sectional views of the beams tested experimentally [15]**

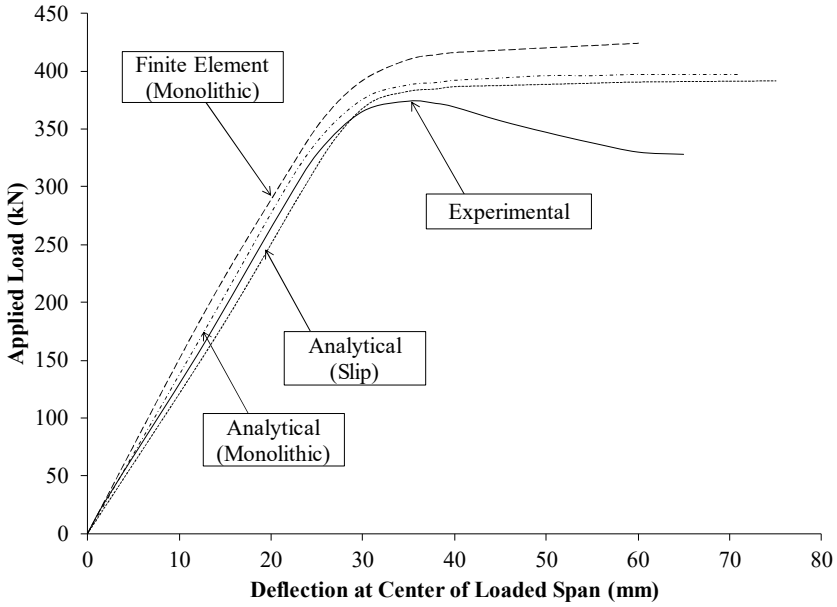


**Figure 7: Validation of the proposed model**

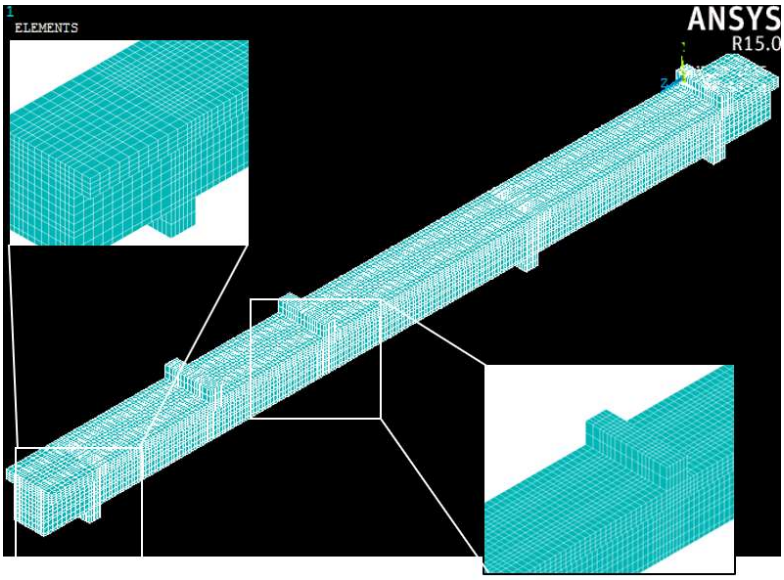


**Figure 8: Meshing of the jacketed beam in ANSYS**

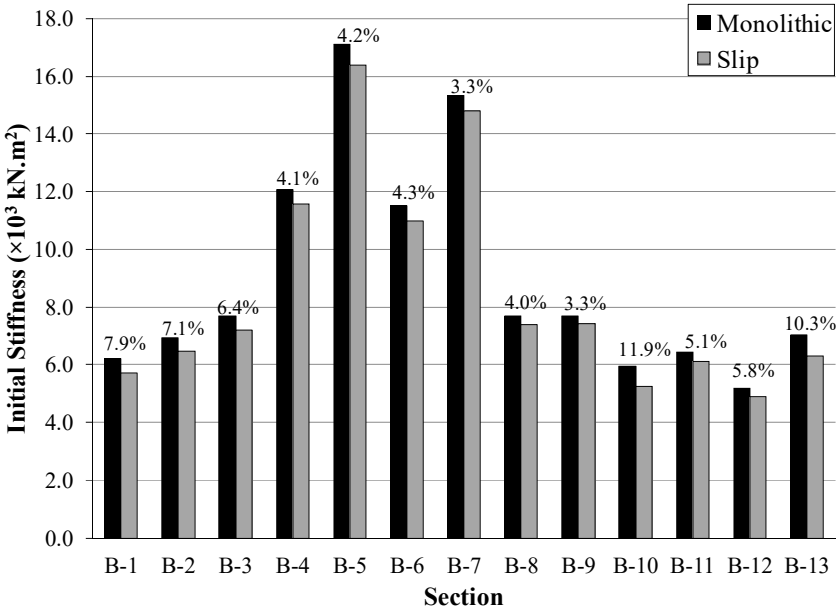


**Figure 9: Percent difference of initial stiffness with and without slip effect (sagging)**

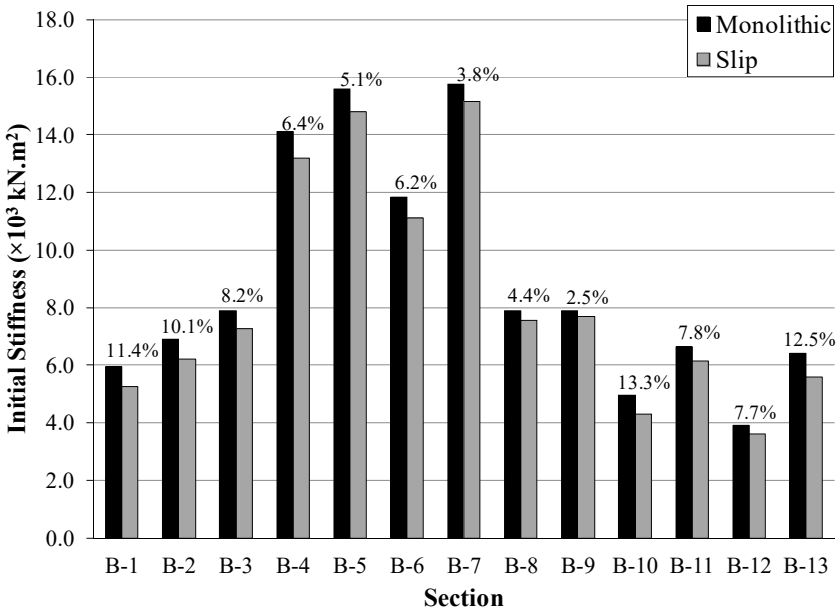


**Figure 10: Percent difference of initial stiffness with and without slip effect (hogging)**

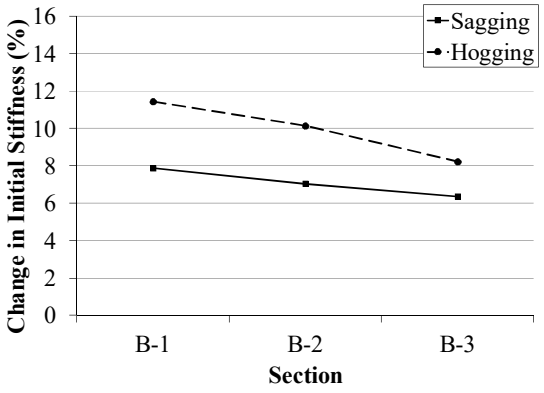


**(a) jacket thickness**

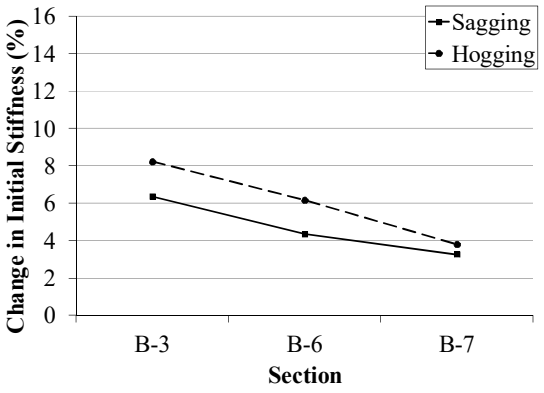


**(b) section width**

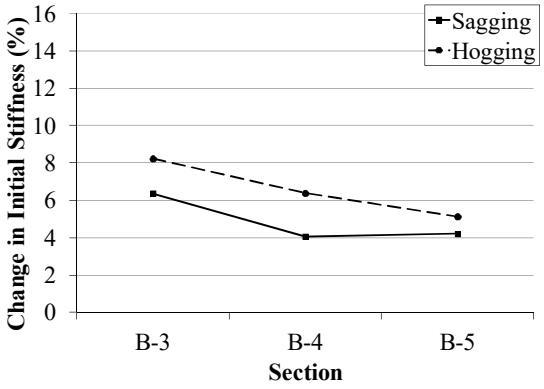


**(c) section height**

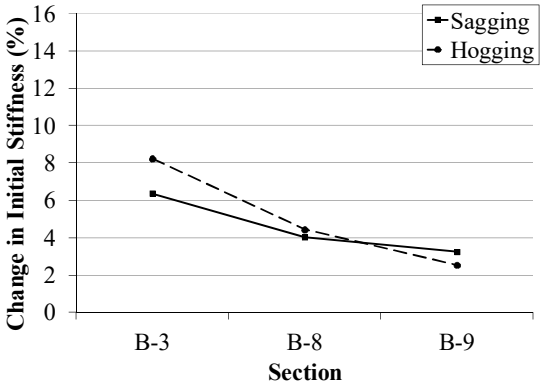


**(d) span**

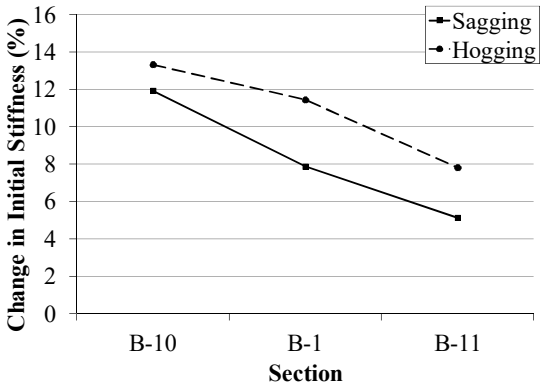


**(e) concrete compressive strength**

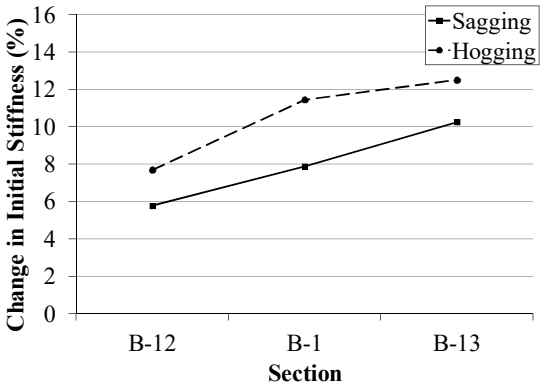


**(f) steel grade**

**Figure 11: Variation of sagging and hogging initial stiffness with various parameters**

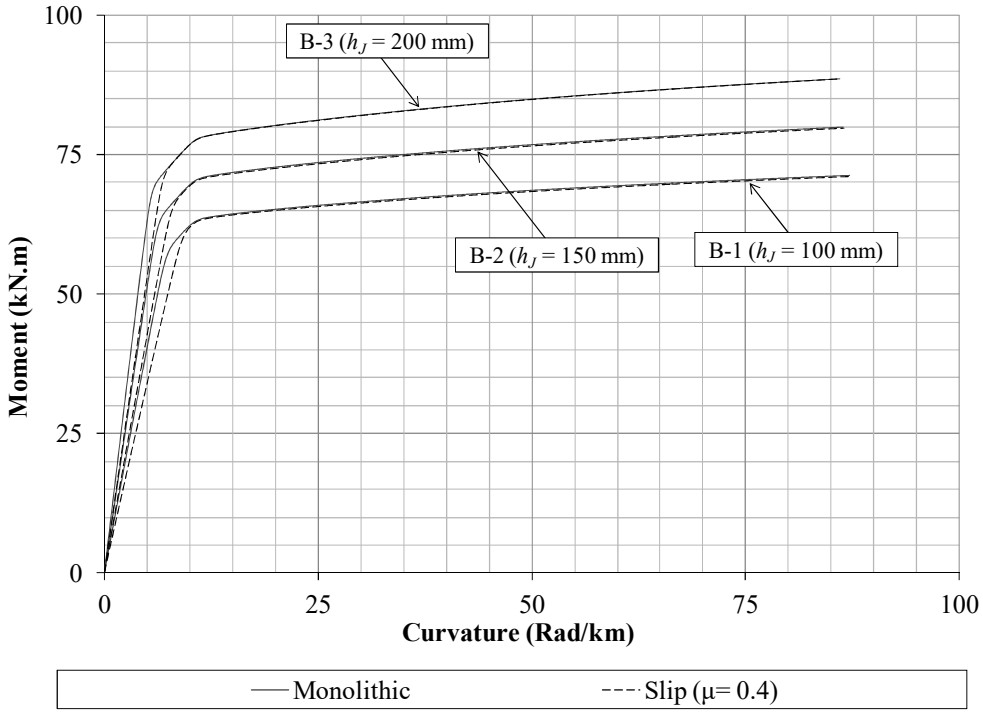


**Figure 12: Effect of varying $h_J$ on the $M$-$\varphi$ relationship (sagging)**

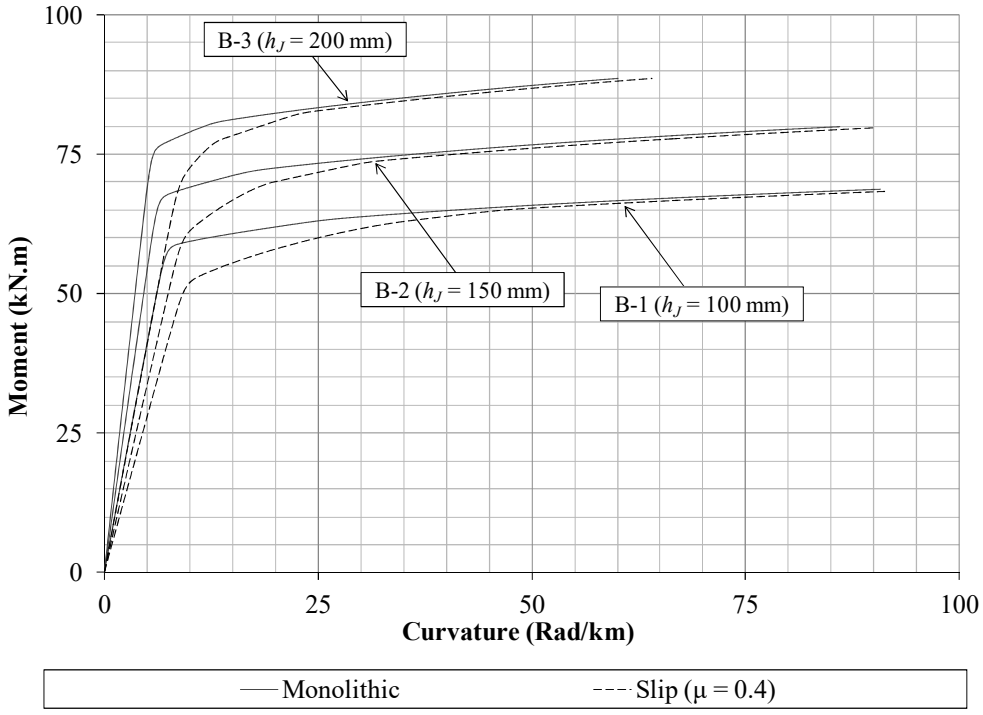


**Figure 13: Effect of varying $h_J$ on the $M$-$\varphi$ relationship (hogging)**

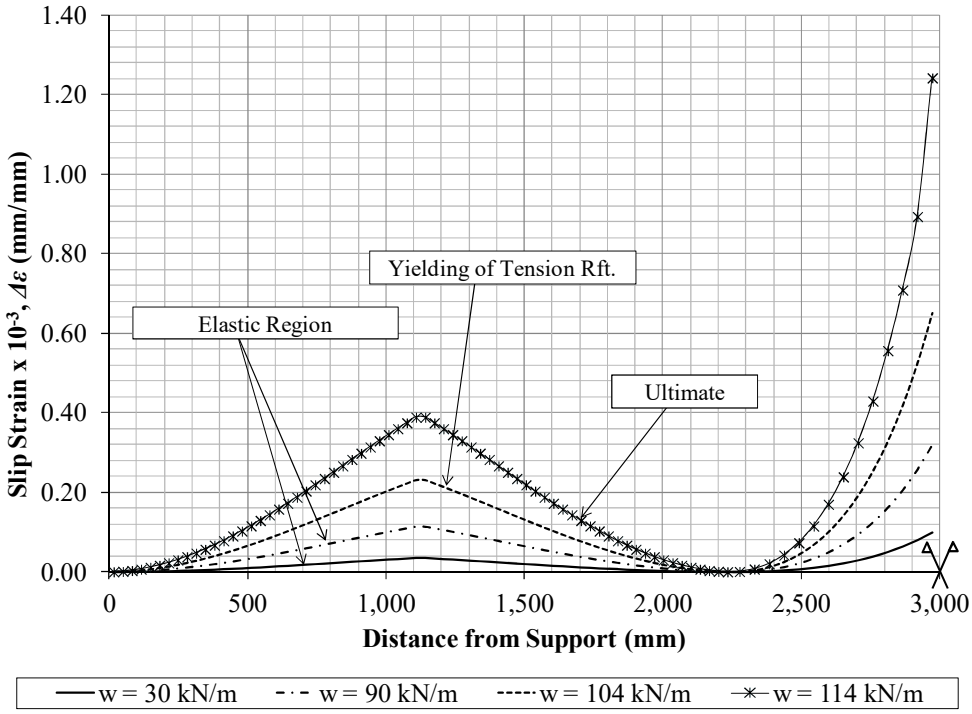


**Figure 14: Slip strain ($\Delta\varepsilon$) distribution along beam B-5 ($\mu$ = 0.4)**

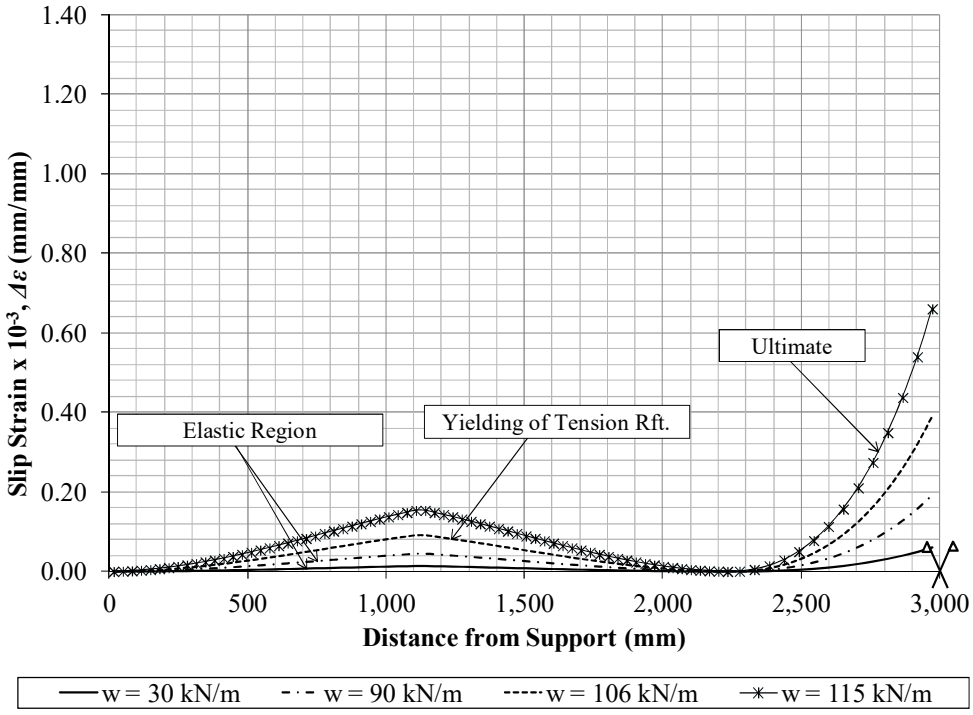


**Figure 15: Slip strain ($\Delta\varepsilon$) distribution along beam B-5 ($\mu$ = 1.0)**

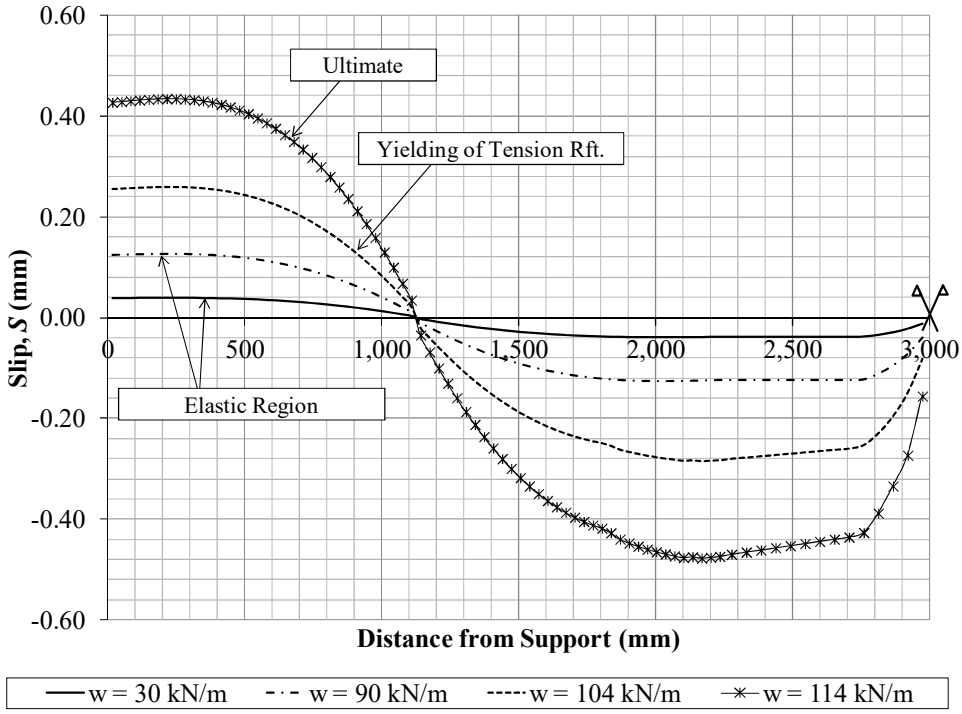


**Figure 16: Slip distribution along beam B-5 ($\mu$ = 0.4)**

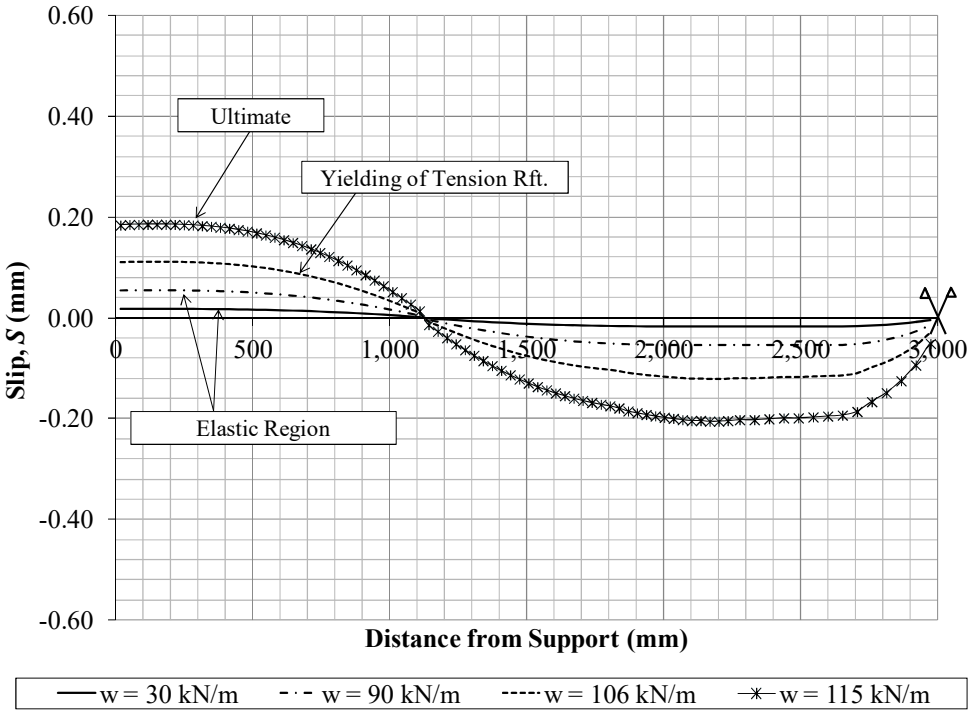


**Figure 17: Slip distribution along beam B-5 ($\mu$ = 1.0)**

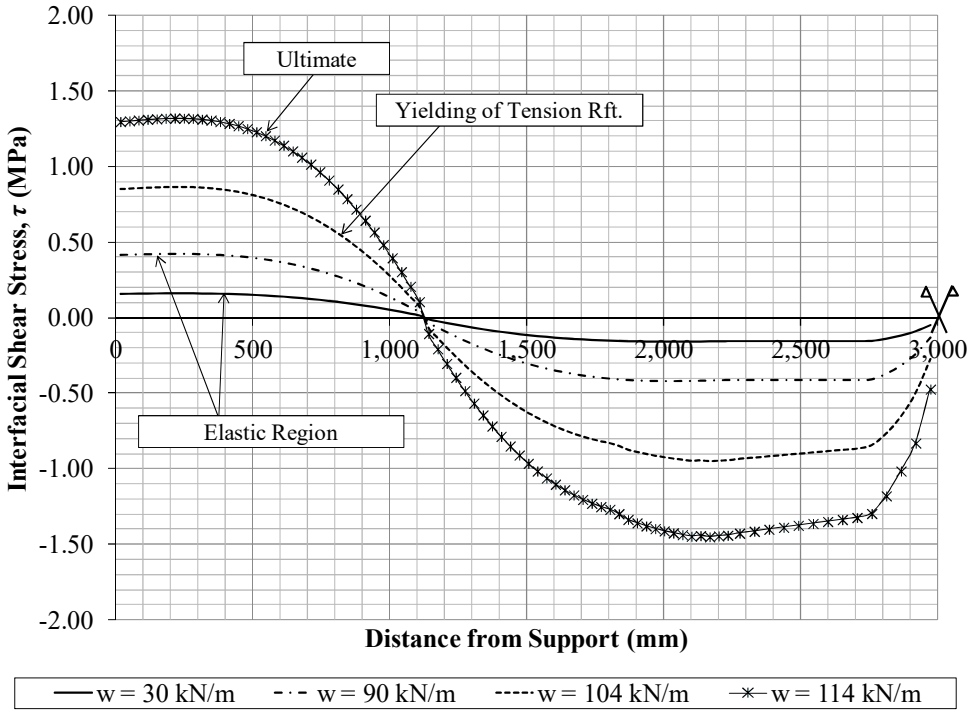


**Figure 18: Interfacial shear stress distribution along beam B-5 ($\mu$ = 0.4)**

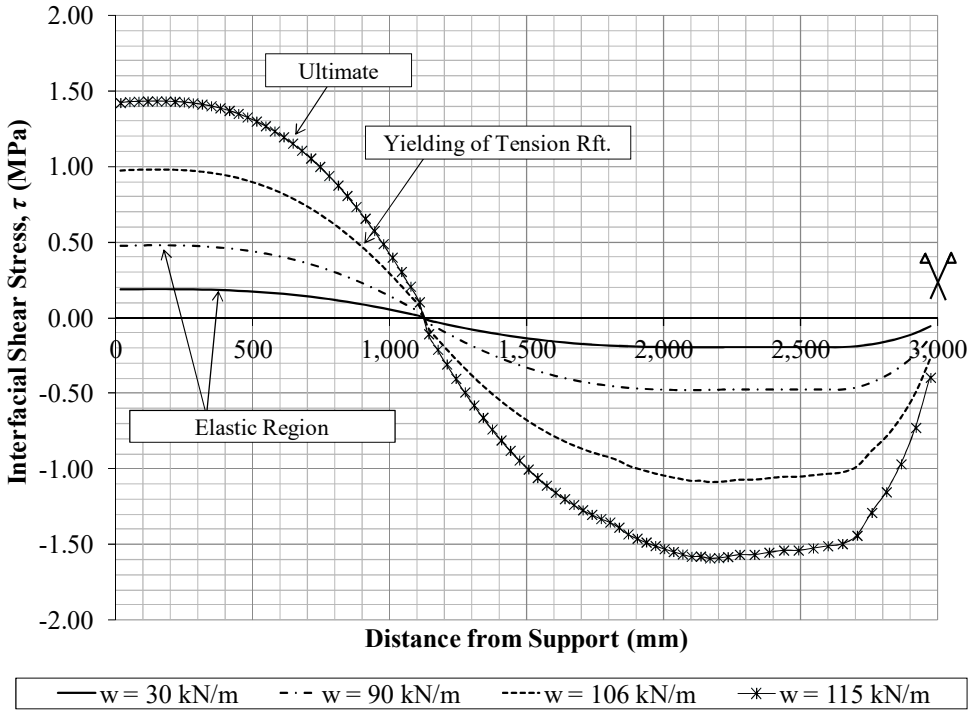


**Figure 19: Interfacial shear stress distribution along beam B-5 ($\mu$ = 1.0)**

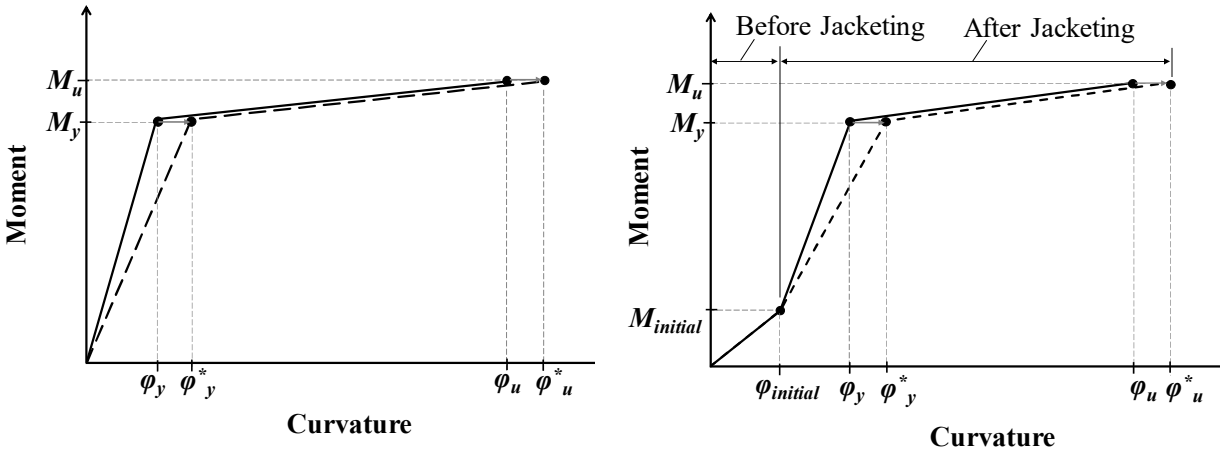


**(a) No initial load.** **(b) With initial load.**

**Figure 20: Typical moment-curvature diagram for jacketed beams.**

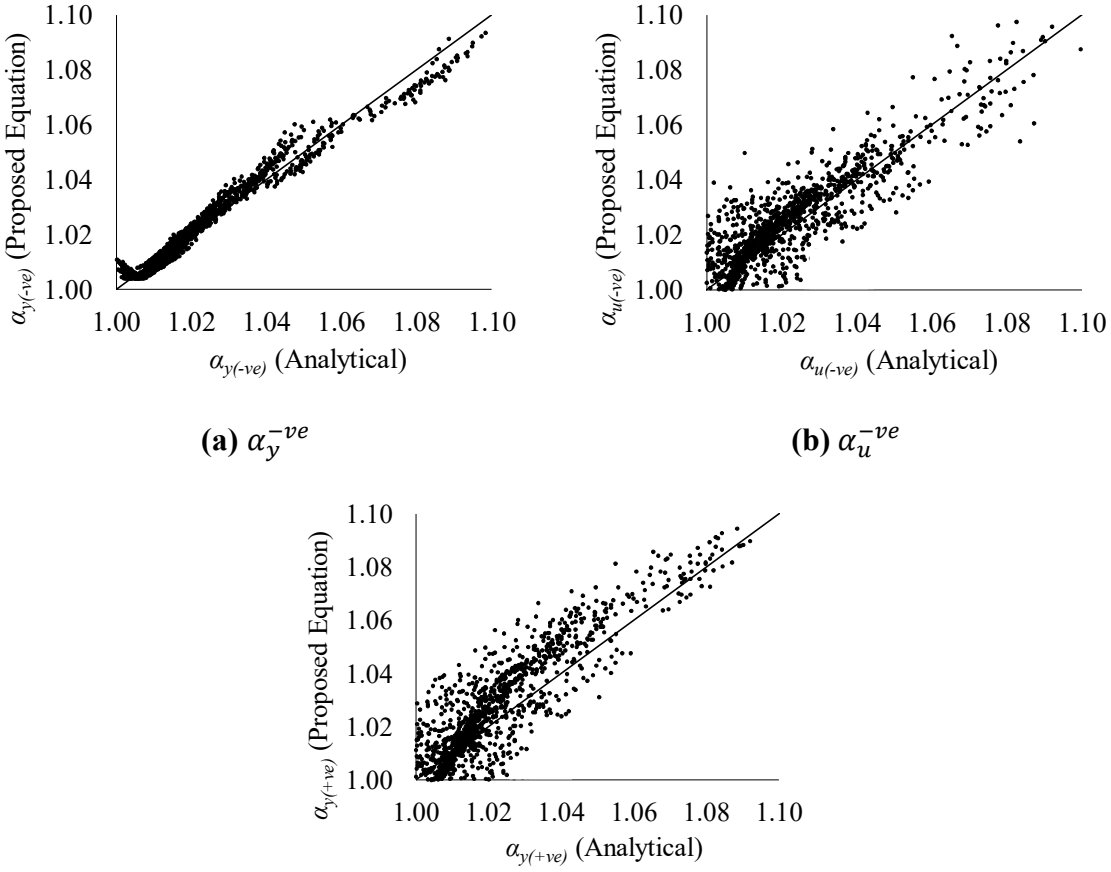


**(a)** $\alpha_y^{-ve}$ **(b)** $\alpha_u^{-ve}$

**(c)** $\alpha_y^{+ve}$

**Figure 21: Statistical analysis for the proposed expressions**

## 13. References


[1] Tassios, T., Vintzeleou, E. "Concrete-to-Concrete Friction," Journal of Structural Engineering, ASCE, 1987, Vol. 113, No. 4, pp. 832-849.

[2] Altun, F. "An experimental study of the jacketed reinforced-concrete beams under bending," Construction and Building Materials, 2004, Vol. 18, No. 8, pp. 611-618.

[3] Bousias, S., Spathis, A. and Fardis, M. "Seismic retrofitting of columns with lap-spliced smooth bars through FRP or concrete jackets," Journal of Earthquake Engineering, 2007, Vol. 11, pp. 653-674.

[4] Santos, P. and Júlio, E. "A State-of-the-Art Review on Shear-Friction," Engineering Structures, 2012, Vol. 45, pp. 435-448.

[5] Martinola, G., Meda, A., Plizzari, G.A. and Zinaldi, Z. "An Application of High Performance Fiber Reinforced Cementitious Composites for RC Beam Strengthening," Fracture Mechanics of Concrete and Structures - High Performance Concrete, Taylor and Francis Group, 2007, pp. 1541-1548.

[6] Shimoyama, Y., Uzawa, M. "Properties and application of ductal," Journal of the Taiheiyo Cement Corporation, 2002, Vol. 142, pp. 55-62.

[7] Vicenzino, E., Culhman, G., Perry, V., Zakariasen, D. and Chow, T. "The first use of UHPFRC in thin precast roof shell for LRT Canadian station," PCI Journal, September- October, 2005.

[8] Li, V.C. "From Micromechanics to Structural Engineering - the design of cementitious composites for civil engineering applications," Doboku Gakkai Rombun-Hokokushu/Proceedings of the Japan Society of Civil Engineers, 1993, Vol. 471, No. 1-24, pp. 1-12.

[9] Rossi, P. “High Performance multimodal fiber reinforced fiber reinforced cement composite (HPMFRCC): the LPC experience,” ACI Materials Journal, 1997, Vol. 94, No. 6, pp. 478-483.

[10] Meda, A., Minelli, F., Plizzari, G.A. and Riva, P. “Shear behavior of steel fiber reinforced concrete beams,” Materials and Structures, 2005, Vol. 38, No. 3, pp. 343-351.

[11] Shehata, I., Shehata, L., Santos, E. and Simoes, M. “Strengthening of Reinforced Concrete Beams in Flexure by Partial Jacketing,” Materials and Structures, 2009, Vol. 42, No. 4, pp. 495-504.

[12] Tsonos, A.D.G. “Performance enhancement of R/C building columns and beam-column joints through shotcrete jacketing,” Engineering Structures, 2010, Vol. 32, pp. 726-740.

[13] Hamilton, C., Pardoen, G., Navalpakkam, S. and Kanzanjy, R. “Reinforced concrete bridge column performance enhancement through shotcrete jacketing,” ACI Structural Journal, 2004, Vol. 101, No. 3, pp. 332-340.

[14] Souza, R.H.F. and Appleton, J. “Flexural Behavior of Strengthened Reinforced Concrete Beams,” Materials and Structures, 1997, Vol. 30, pp. 154-159.

[15] Cheong, H.K. and MacAlevey, N. “Experimental Behavior of Jacketed Reinforced Concrete Beams,” Journal of Structural Engineering – ASCE, 2000, Vol. 126, No. 6, pp. 692-699.

[16] Alhadid, M.M. and Youssef, M.A. “Analysis of reinforced concrete beams strengthened using concrete jackets,” Engineering Structures, Elsevier, 2017, Vol. 132, pp. 172-187.

[17] Scott, B.D., Park, R. and Priestley, M.J.N. “Stress-Strain Behavior of Concrete Confined by Overlapping Hoops at Low and High Strain Rates,” Journal of the American Concrete Institute, 1982, Vol. 79, No. 1, pp. 13-27.

[18] Karthik, M.M and Mander, J.B. "Stress-block parameters for unconfined and confined concrete based on a unified stress-strain model," Journal of Structural Engineering – ASCE, 2011, Vol. 137, No. 2, pp. 270-273.

[19] Ramberg, W. and Osgood, W.R. "Description of stress–strain curves by three parameters," Technical Note No. 902, National Advisory Committee for Aeronautics, 1943, Washington DC.

[20] Thermou, G.E., Pantazopoulou, S.J. and Elnashai, A.S. "Flexural behavior of brittle RC members rehabilitated with concrete jacketing," Journal of Structural Engineering, ASCE, 2007, Vol. 133, No. 10, pp. 1373-1384.

[21] CSA. "Design of concrete structures (CAN/CSA A23.3-14)," Cement Association of Canada, 2014, Ottawa, ON.

[22] Tsioulou, O.T. and Dritsos, S.E. "A theoretical model to predict interface slip due to bending," Materials and Structures, 2011, Vol. 44, pp. 825-843.

[23] Kotsira, E., Dritsos, S., Pilakoutas, K. "Effectiveness of techniques for flexural repair and strengthening of RC members," Proceedings of the 5th international conference on Structural faults and repair, 1993, Edinburgh, UK, pp. 235-243.

[24] Saiidi, M., Vrontinos, S. and Douglas, B. "Model for the response of reinforced concrete beams strengthened by concrete overlays," ACI Structural Journal, 1990, Vol. 87, No. 6, pp. 687-695.

[25] Youssef, M.A. and Rahman, M. "Simplified seismic modeling of reinforced concrete flexural members," Magazine of Concrete Research, 2007, Vol. 59, No. 9, pp. 639-649.

[26] Kassimali, A. "Matrix Analysis of Structures," Thomson-Engineering, 2nd ed., 2011, 640 pp.

[27] Oehlers, D.J., Haskett, M., Mohamed, M.S. and Griffith, M.C. “Moment Redistribution in Reinforced Concrete Beams,” Proceedings of the Institution of Civil Engineers, Structures and Buildings 163, June 2010, pp. 165-176.

[28] ACI Committee 318. “Building code requirements for structural concrete and commentary (ACI 318-14),” American Concrete Institute, 2014, Farmington Hills, MI.